Journal of Power Sources 252 (2014) 164–168

Contents lists available at ScienceDirect

Journal of Power Sources

journal homepage: www.elsevier.com/locate/jpowsour

Short communication

Novel metal-supported solid oxide fuel cells with impregnated symmetric $La_{0.6}Sr_{0.4}Fe_{0.9}Sc_{0.1}O_{3-\delta}$ electrodes

Yucun Zhou, Xuejiao Liu, Junliang Li, Huaiwen Nie, Xiaofeng Ye, Shaorong Wang*, Zhongliang Zhan*

CAS Key Laboratory of Materials for Energy Conversion, Shanghai Institute of Ceramics, Chinese Academy of Sciences (SICCAS), 1295 Ding-xi Road, Shanghai 200050, China

HIGHLIGHTS

- Novel metal-supported SOFCs are fabricated by tape casting and co-sintering.
- LSFSc oxides are used as symmetric electrode catalysts by impregnation method.
- Nano-scale LSFSc catalysts are highly active for electrodes reactions.

ARTICLE INFO

Article history:
Received 13 July 2013
Received in revised form
4 December 2013
Accepted 5 December 2013
Available online 14 December 2013

Keywords:
Metal-supported solid oxide fuel cells
Symmetric electrodes
Impregnation
Nanostructures

ABSTRACT

This paper reports on the fabrication of novel metal-supported solid oxide fuel cells containing porous 430L stainless steel substrates, YSZ electrolytes and porous YSZ cathode backbones. Such tri-layer structures are obtained by the tape casting, lamination and co-firing techniques. Redox-stable $La_{0.6}Sr_{0.4}Fe_{0.9}Sc_{0.1}O_{3-\delta}$ (LSFSc) oxides are introduced as symmetric electrode catalysts onto the internal surfaces of porous 430L substrates and YSZ backbones using the solution impregnation method. The maximum power density is 0.65 W cm^{-2} measured at 800 °C. Impedance analyses show that the anode polarizations are the largest losses while the cathode polarizations make negligible contribution to the total cell resistances.

1. Introduction

Metal-supported solid oxide fuel cells (MS-SOFCs) use the electrically conductive and mechanically robust alloys to support the electrochemically active components (including anodes, electrolytes and cathodes) and show important advantages over the common all-ceramic counterparts such as excellent structural robustness and stability, high tolerance toward rapid thermal cycling, easy stack assembling as well as low materials costs [1]. Due to their low costs, compatible thermal expansion coefficients with the standard yttria-stabilized zirconia (YSZ) electrolytes and adequate resistances against high temperature oxidation, ferritic FeCr stainless steels have been most commonly used as the metallic substrates [2]. Nevertheless, adoption of ferritic stainless steels as the mechanic supports for MS-SOFCs complicated the fabrication procedure and necessitated operation at reduced temperatures. For example, atomic inter-diffusion occurred between ferritic FeCr substrates and nickel-containing anodes for co-fired MS-SOFCs. Diffusion of iron and chromium from ferritic substrates into nickel-anodes might substantially decrease their catalytic activities for hydrogen oxidation reactions. In the meanwhile, diffusion of nickel from anodes into substrates could alter their mechanic properties and may increase their thermal expansion coefficients [3,4]. Furthermore, application of cathode layers is also challenging for MS-SOFCs since the commonly used cathode materials such as $La_{1-x}Sr_xMnO_{3-\delta}$ (LSM) and $La_{1-x}Sr_xCo_{1-y}Fe_yO_{3-\delta}$ (LSCF) would decompose when sintered at high temperatures in the reducing atmosphere that is required to prevent excessive oxidation of stainless steel substrates [5]. In-situ sintering has been used to fabricate the cathode layers during the fuel cell operation [6,7], but might be problematic in terms of technically reliability and long-term durability [8].

* Corresponding authors. Tel./fax: +86 21 6990 6373.
E-mail addresses: srwang@mail.sic.ac.cn (S. Wang), zzhan@mail.sic.ac.cn (Z. Zhan).

0378-7753/$ – see front matter © 2013 Elsevier B.V. All rights reserved.
http://dx.doi.org/10.1016/j.jpowsour.2013.12.020

Impregnation has shown great promise for fabricating high performance metal-supported SOFCs. Since the active electrode catalysts were introduced into the pre-sintered backbones at relatively low temperatures, issues such as atomic inter-diffusion that would otherwise occur at the co-firing temperature could be effectively avoided. Furthermore, the resulting nano-scale catalysts allow for superior catalytic activities for hydrogen oxidation or oxygen reduction reactions, decreasing the interfacial polarization resistances and increasing the fuel cell power densities [9]. For example, MS-SOFCs with impregnated Ni–YSZ anode and LSM–YSZ cathode showed power density of 0.33 W cm^{-2} at 700 °C [10]. Recently, we showed that $La_{0.6}Sr_{0.4}Fe_{0.9}Sc_{0.1}O_{3-\delta}$ (LSFSc) exhibited good structural stability and reasonable conductivities in both oxidizing and reducing atmospheres (*e.g.*, 100 S cm^{-1} in air and 0.7 S cm^{-1} in 97% H_2–3% H_2O at 800 °C), and that the impregnated LSFSc catalysts demonstrated high catalytic activities for both oxygen reduction and hydrogen oxidation reactions [11]. Nevertheless, co-impregnation of copper as the current collecting layer was required in order for LSFSc catalysts to function well as the anodes due to their low conductivities in hydrogen atmospheres. Here we report the design of impregnated LSFSc–430L composites as the anodes for MS-SOFCs that combine advantages of high electronic conductivities from the supporting 430L alloy substrates and of good catalytic activities from the impregnated LSFSc catalysts for hydrogen oxidation reactions. Based upon the good structural stability in reducing atmospheres, LSFSc particles are also impregnated into the porous YSZ backbones and simultaneously act as the cathode catalysts. The use of redox-stable LSFSc oxides as the symmetric electrode catalysts might be able to eliminate complicated issues with MS-SOFCs such as nickel coarsening, metallic diffusion and poor interfacial bonding between the cathode and the electrolyte.

2. Experimental

The metal-supported SOFCs were based upon tri-layer structures of porous 430L substrates|YSZ electrolytes|porous YSZ backbones, which were fabricated by the tape casting, tape lamination and co-firing methods. Commercial 430L stainless steel powders (Jing-yuan Powder Material Co., Ltd, China) and 8YSZ (Tosoh, Japan) were used as starting materials. The slurry for tape casting was ethanol-based and consisted of acrylic resin dispersants, polyvinyl butyral binders, dibutyl phthalate plasticizer and other organic additives in addition to alloy or ceramic powders. Green tapes were obtained by casting appropriate slurries on the Mylar carrier on the tape casting machine (Lab-Cast Model TC-71LC Tape Caster, HED International, USA). The tri-layers were produced by laminating tape cast green tapes followed by co-sintering at 1300 °C for 4 h in 5% H_2–95% N_2. LSFSc catalysts were introduced into the porous 430L and YSZ backbones by impregnating aqueous solutions containing stoichiometric amounts of $La(NO_3)_3$, $Sr(NO_3)_2$, $Fe(NO_3)_3$ and $Sc(NO_3)_3$ (99% pure, Sinopharm Chemical Reagent), where citric acid (99% pure, Sinopharm Chemical Reagent) was added at a 1:1 M ratio of citric acid to metal ions. After drying at 80 °C, heat treatment was conducted at 850 °C in humidified 5% H_2–95% N_2 for 2 h to promote formation of LSFSc perovskite oxides without oxidizing 430L substrates. The amount of deposited LSFSc catalysts during each impregnation cycle was controlled by a micro-liter syringe and the impregnation/heat treatment cycles were repeated to increase the amounts of deposited catalysts. Symmetric anode and cathode fuel cells were prepared similarly, based upon porous 430L|YSZ electrolyte|porous 430L and porous YSZ|YSZ electrolyte|porous YSZ, respectively.

For electrochemical measurements, silver grids were applied on the electrode surfaces with silver wires attached as the voltage and current leads. Single fuel cells were sealed onto alumina tubes using silver paste (DAD-87, Shanghai Research Institute of Synthetic Resins), and current–voltage curves were obtained using an IM6 Electrochemical Workstation (ZAHNER, Germany) at 650–800 °C with cathodes exposed to air and anodes to humidified (3% H_2O) hydrogen at 100 sccm. Electrochemical impedance spectra (EIS) were collected at open circuits with 20 mV AC amplitudes over the frequency range of 50 mHz–0.2 MHz.

Phase compositions of the impregnated LSFSc catalysts were determined at room temperature using a Rigaku XRD diffractometer with monochromatic CuK_α radiation. The microstructures of metal-supported SOFCs were examined using scanning electron microscopy (SEM) in the S-4800-II microscope. The porosity and pore-size distribution of porous 430L substrates and YSZ backbones were measured using mercury intrusion porosimetry carried out with a Micromeritics AutoPore IV 9500 V1.09.

3. Results and discussion

Fig. 1a shows a representative cross-sectional SEM micrograph of single MS-SOFCs after the fuel cell measurement, consisting of porous LSFSc impregnated 430L anode substrates, YSZ electrolytes and porous LSFSc impregnated YSZ cathodes. The YSZ electrolyte layers were fully dense with a typical thickness of ≈25 μm, and were well bonded with the adjacent 430L substrates and porous YSZ backbones. Based upon the mercury porosimetry measurements, the porosities for the 430L and YSZ backbones prior to any impregnation were 44 and 69% with a mean pore size at 17 and 1 μm, respectively. Higher-magnification micrographs are shown in Fig. 1b for the impregnated LSFSc–YSZ cathodes at loadings of 30 wt% and in Fig. 1c for the impregnated LSFSc–430L anodes at loadings of 10 wt%. Both electrodes exhibited well inter-connected LSFSc particles along the pore walls of the supporting backbones, which was critically important to maximize the active zones for electrochemical reactions by reducing the number of isolated catalysts [10,12]. Fig. 1a–c also show that highly porous microstructures were well maintained after impregnating 10 wt% LSFSc catalysts into the porous 430L substrates and 30 wt% LSFSc catalysts into the porous YSZ backbones. Further increase in the catalysts loadings resulted in decreased porosities for both electrodes and increased gas diffusion resistances. Fig. 1d shows a nanoporous structure for the impregnated LSFSc particles with average particle sizes and mean pore sizes both at about 100–200 nm, as typically produced via calcination of infiltrate solutions at 850 °C [13,14].

To confirm the formation of perovskite LSFSc oxide catalysts, X-ray diffraction measurements were performed on the impregnated electrodes with results shown in Fig. 2a for LSFSc–430L composites and in Fig. 2b for LSFSc–YSZ composites. In addition to the dominant diffraction peaks from the supporting 430L or YSZ backbones, some small peaks were observed at 32.2, 39.7, 46.1 and 57.4, which indicated that phase-pure LSFSc oxides formed after calcinations in humidified 5% H_2–95% N_2 at 850 °C. In order to better observe X-ray diffraction patterns of these infiltrates without interference from the supporting backbones, the infiltrate solutions were gelated and dried at 80 °C, followed by calcinations at 850 °C in humidified 5% H_2–95% N_2. XRD patterns shown in Fig. 2c indicated that the resulting powders were well crystallized in the perovskite structure. In consistency with our prior report [11], further heat-treatment in a more reducing environment of 97% H_2–3% H_2O at 800 °C for 10 h resulted in an expansion in the lattice parameter, but did not substantially alter the perovskite structure with a rhombohedral symmetry (Fig. 2d). Such enhanced stability has previously been reported for Sc-doped $La_{0.8}Sr_{0.2}MnO_3$ oxides [5].

Electrochemical measurements were performed on the MS-SOFCs with humidified hydrogen fuels and air oxidants at 650–

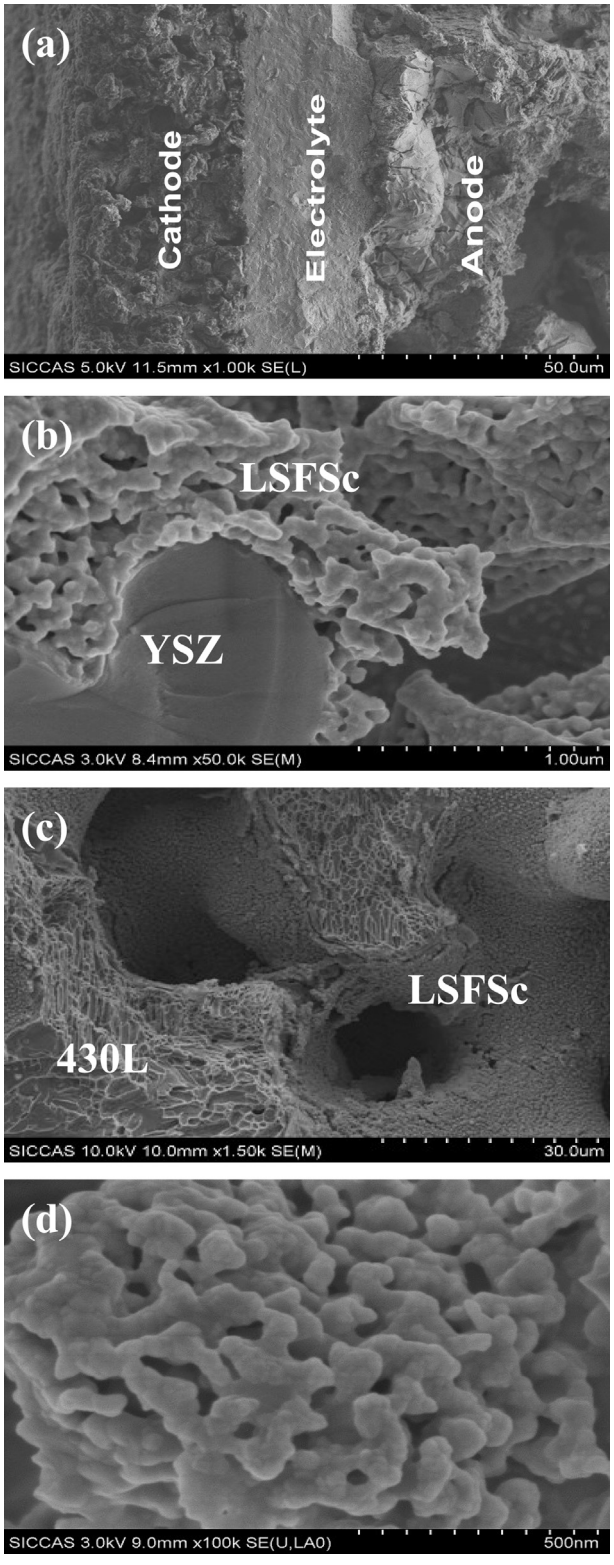

Fig. 1. (a) Cross-sectional scanning electron microscope (SEM) images of the metal-supported SOFCs after fuel cell measurements, (b) high-magnification SEM micrograph of impregnated LSFSc–YSZ cathodes, (c) High-magnification SEM micrograph of impregnated LSFSc–430L anodes and (d) higher-magnification SEM micrograph of impregnated LSFSc particles shown in (b).

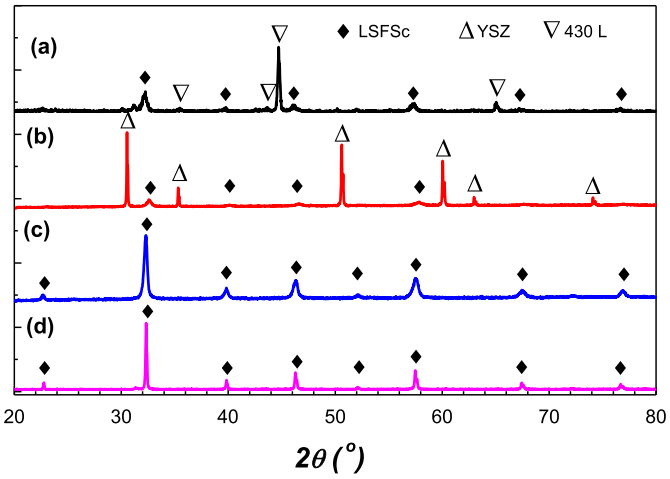

Fig. 2. X-Ray diffraction patterns of (a) LSFSc–430L anodes at loadings of 10 wt%, (b) LSFSc–YSZ cathodes at loadings of 30 wt%, (c) LSFSc powders synthesized in humidified 5% H_2–95% N_2 at 850 °C, and (d) LSFSc powders reduced in 97% H_2–3% H_2O at 800 °C for 10 h.

800 °C with typical cell voltages and power densities as a function of current densities shown in Fig. 3a. The open circuit voltage was 1.06 V at 800 °C and was within 50 mV of the thermodynamically expected Nernst potentials, indicating excellent impermeability of YSZ electrolyte thin films shown in Fig. 1a. The maximum power densities measured were 0.18, 0.30, 0.42 and 0.65 W cm^{-2} at 650, 700, 750 and 800 °C, respectively. Notwithstanding the use of ceramic oxides as the anode catalysts that are usually less active for

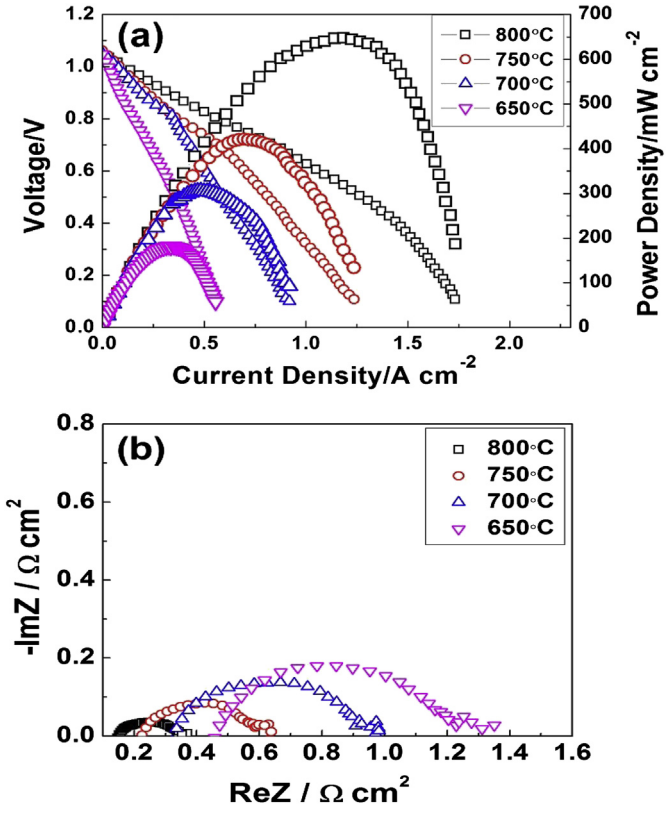

Fig. 3. (a) Current–voltage characteristics of the present MS-SOFCs operating on hydrogen fuels and air oxidants at 650–800 °C and (b) impedance spectra measured at open circuits.

hydrogen oxidation reactions than the standard nickel anodes, power densities for the present MS-SOFCs were much higher than for co-fired FeCr alloy supported Ni–YSZ anode and YSZ electrolyte fuel cells [2], and were comparable with those reported for MS-SOFCs with plasma sprayed Ni–YSZ anodes [15] or impregnated Ni–YSZ anodes [10]. Fig. 3b shows Nyquist plots of impedance data obtained at open circuits for the present MS-SOFCs. All plots featured large high-frequency arcs and small low-frequency arcs, where the former increased much more pronouncedly than the latter with decreasing temperature. The combined interfacial polarization resistances, taken from the overall widths of the two depressed arcs, were 0.20, 0.43, 0.66 and 0.84 Ω cm^2 at 800, 750, 700 and 650 °C, respectively.

In order to determine the individual contributions of the cathode and the anode to the combined interfacial polarization resistances, impedance measurements were also performed for symmetric cathode fuel cells in air and for symmetric anode fuel cells in 97% H_2–3% H_2O. Representative Nyquist plots at 800 °C are shown in Fig. 4a for the cathode and in Fig. 4b for the anodes, where the ohmic losses due to the electrolytes were removed and the interfacial polarization resistances were divided by two so as to account for contributions from two symmetric electrodes. Fig. 4c compares Bode plots of the impedance data taken in air and in hydrogen at 800 °C. Notably, oxygen reduction kinetics was largely dominated by charge transfer along the YSZ|LSFSc interfaces with the summit relaxation frequency at 1 kHz, while the surface oxygen exchange process was quick enough and made little contributions to the cathode polarization resistance since the arc commonly centered at 1–10 Hz was negligible small [14]. Fig. 4b shows that hydrogen oxidation kinetics at 800 °C was co-limited by charge transfer reactions and the surface hydrogen exchange process that had summit relaxation frequencies at 1 kHz and 3 Hz, respectively. Nevertheless, the low-frequency arc in Fig. 4b did not change significantly while the high-frequency arc increased exponentially and became dominant at lower temperatures.

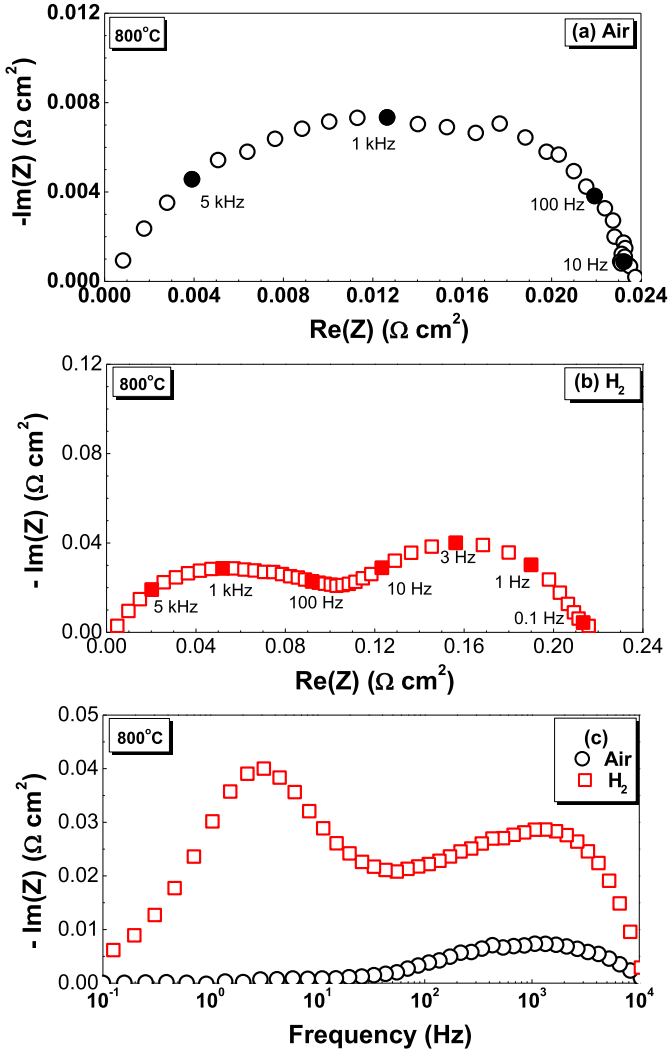

Fig. 4. Representative Nyquist plots of impedance spectra measured at 800 °C for (a) symmetrical cathode fuel cells in dry air and (b) symmetrical anode fuel cells in 97% H_2–3% H_2O and (c) comparison of Bode plots for the impedance data shown in (a) and (b).

Fig. 4a also shows that the cathode polarization resistance was $R_{P,C} = 0.024\ \Omega\ cm^2$ in air, which was comparable to previously reported values for impregnated $La_{0.8}Sr_{0.2}Co_{0.5}Fe_{0.5}O_3$ (LSCF)– or $La_{0.8}Sr_{0.2}FeO_3$ (LSF)–YSZ composites (Table 1) [16,17]. These results indicate that scandium substitution for ferric in the perovskite oxides did not adversely affect their catalytic activity for oxygen reduction reactions even though the electrical conductivities became a little bit smaller. Fig. 4b shows that the anode polarization resistance was $R_{P,A} = 0.21\ \Omega\ cm^2$, which was reasonably small given the inertness of the 430L supporting backbones for hydrogen oxidation reactions. In contrast, the impregnated $La_{0.6}Sr_{0.4}Fe_{0.9}Sc_{0.1}O_{3-\delta}$–$La_{0.9}Sr_{0.1}Ga_{0.8}Mg_{0.2}O_{3-\delta}$ (LSFSc–LSGM) composites produced an anode polarization resistance of 0.89 Ω cm^2 in humidified hydrogen at 800 °C, which decreased dramatically to 0.28 Ω cm^2 by improving current collection via an additionally impregnated copper layer [11]. The $R_{P,A}$ value for the present LSFSc–430L composite was approximately 30% smaller than for the co-impregnated Cu-LSFSc–LSGM composite. Therefore, quick electron transport was critically important for hydrogen oxidation reactions on the LSFSc catalysts. Note that the impregnated LSFSc–430L composite anodes also showed substantially smaller polarization resistances than prior alternative oxide anodes (Table 1), *e.g.*, 0.43 Ω cm^2 for $Mn_{1.5}Co_{1.5}O_4$ impregnated YSZ anodes at 800 °C [18], 5.1 Ω cm^2 for CeO_2 impregnated FeCr alloy–YSZ cermet and 1.2 Ω cm^2 for $Ce_{0.8}Gd_{0.2}O_{2-\delta}$ (GDC) impregnated FeCr alloy–YSZ cermet at 650 °C [19].

Fig. 5 summarizes the anode and cathode polarization resistances at varied temperatures. Included for comparison were the pure ohmic (R_o) losses for the present MS-SOFCs as taken from the high-frequency real-axis intercepts of Nyquist plots shown in Fig. 3b, which were 0.15, 0.21, 0.32 and 0.47 Ω cm^2 at 800, 750, 700 and 650 °C, respectively. Based on the oxide ionic conductivity value of 0.03 S cm^{-1}, the electrolyte resistance for a 25 μm-thick YSZ layer was $R_{EL} = 0.083\ \Omega\ cm^2$ at 800 °C. Higher than expected R_o values indicated that there were additional losses other than the electrolyte resistances, which may be due to non-optimized current collection in the cathodes. Fig. 5 showed that the anode polarization resistances were approximately 5–10 times higher than the cathode polarization resistances and were the dominant losses at all temperatures for the present MS-SOFCs. In particular, the anode

Table 1
Comparison of polarization resistances (R_p) of impregnated electrodes.

Impregnated electrodes	Temperature (°C)	R_p (Ω cm^2)
LSCF impregnated YSZ cathode	750	0.047 [16]
LSF impregnated YSZ cathode	700	0.1 [17]
LSFSc impregnated LSGM anode	800	0.89 [11]
Cu-LSFSc impregnated LSGM anode	800	0.28 [11]
$Mn_{1.5}Co_{1.5}O_4$ impregnated YSZ anode	800	0.43 [18]
CeO_2 impregnated FeCr–YSZ anode	650	5.1 [19]
GDC impregnated FeCr–YSZ anode	650	1.2 [19]

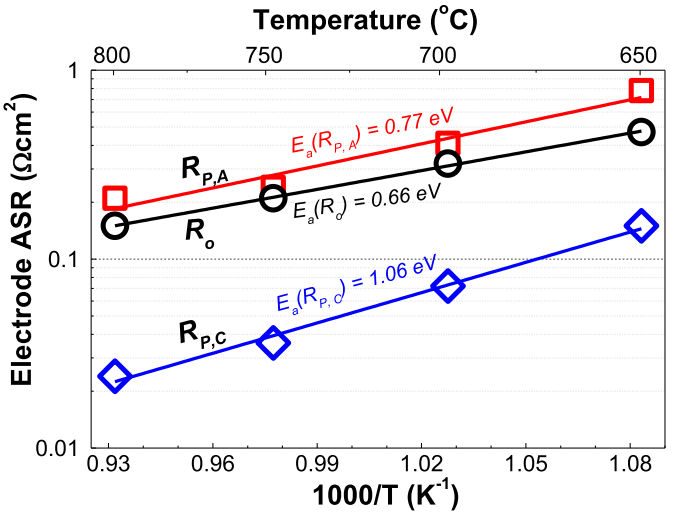

Fig. 5. The pure ohmic losses (R_o) and the polarization resistances for the LSFSc–430L anodes ($R_{P,A}$) and the LSFSc–YSZ cathodes ($R_{P,C}$) plotted versus inverse temperature.

polarization resistances increased from 0.21 to 0.78 Ω cm^2 while the cathode polarization resistances increased from 0.024 to 0.15 Ω cm^2 with decreasing temperature from 800 to 650 °C. The activation energies were 0.77 eV for hydrogen oxidation on impregnated LSFSc–430L anodes and 1.06 eV for oxygen reduction on impregnated LSFSc–YSZ cathodes.

4. Conclusions

In summary, tri-layers of porous 430L substrates|dense YSZ electrolytes|porous YSZ backbones are prepared by tape casting, lamination and co-sintering techniques. Redox-stable LSFSc oxides are impregnated onto the internal surfaces of both 430L and YSZ backbones by solution impregnations with subsequent calcinations in reducing environments at 850 °C. The resulting metal-supported fuel cell yields a maximum power density of 0.65 W cm^{-2} measured at 800 °C. Impedance measurements on symmetric fuel cells indicate that the anode and cathode polarization resistances are 0.21 and 0.024 Ω cm^2 800 °C, indicating that the nano-scale LSFSc catalysts are highly active for both hydrogen reduction and oxygen reduction reactions.

Acknowledgment

We gratefully acknowledge the financial support from National Basic Research Program of China (No. 2012CB215401), the National Natural Science Foundation of China (No. 51172266, 51072219, 51106173, 51071169), Chinese Government High Tech Developing Project (2011AA050702), Science and Technology Commission of Shanghai Municipality and Zhejiang Province under contract No. 11PJ141030 and No. 2011C16037.

References

[1] M.C. Tucker, J. Power Sources 195 (2010) 4570–4582.
[2] I. Villarreal, C. Jacobson, A. Leming, Y. Matus, S. Visco, L. De Jonghe, Electrochem. Solid State Lett. 6 (2003) A178–A179.
[3] M. Brandner, M. Bram, J. Froitzheim, H.P. Buchkremer, D. Stover, Solid State Ionics 179 (2008) 1501–1504.
[4] T. Franco, K. Schibinger, Z. Ilhan, G. Schiller, A. Venskutonis, in: K. Eguchi, S.C. Singhai, H. Yokokawa, H. Mizusaki (Eds.), Solid Oxide Fuel Cells, vol. 10, 2007, pp. 771–780.
[5] Y. Zheng, R. Ran, Z. Shao, Rare Met. 28 (2009) 361–366.
[6] R. Hui, J.O. Berghaus, C. Deces-Petit, W. Qu, S. Yick, J.-G. Legoux, C. Moreau, J. Power Sources 191 (2009) 371–376.
[7] Y.-M. Kim, P. Kim-Lohsoontorn, S.-W. Baek, J. Bae, Int. J. Hydrogen Energy 36 (2011) 3138–3146.
[8] S.-W. Baek, J. Jeong, Y.-M. Kim, J.H. Kim, S. Shin, J. Bae, Solid State Ionics 192 (2011) 387–393.
[9] Y. Zhou, X. Meng, X. Ye, J. Li, S. Wang, Z. Zhan, J. Power Sources 247 (2014) 556–561.
[10] M.C. Tucker, G.Y. Lau, C.P. Jacobson, L.C. DeJonghe, S.J. Visco, J. Power Sources 171 (2007) 477–482.
[11] X. Liu, D. Han, Y. Zhou, X. Meng, H. Wu, J. Li, F. Zeng, Z. Zhan, J. Power Sources 246 (2014) 457–463.
[12] J.M. Vohs, R.J. Gorte, Adv. Mater. 21 (2009) 943–956.
[13] Z.L. Zhan, D. Han, T.Z. Wu, X.F. Ye, S.R. Wang, T.L. Wen, S. Cho, S.A. Barnett, RSC Adv. 2 (2012) 4075–4078.
[14] D. Han, X.J. Liu, F.R. Zeng, J.Q. Qian, T.Z. Wu, Z.L. Zhan, Sci. Rep. UK 2 (2012).
[15] A. Ansar, P. Szabo, J. Arnold, Z. Ilhan, D. Soysal, R. Costa, A. Zagst, M. Gindrat, T. Franco, in: S.C. Singhal, K. Eguchi (Eds.), Solid Oxide Fuel Cells, vol. 12, 2011, pp. 147–155.
[16] J. Chen, F.L. Liang, L.N. Liu, S.P. Jiang, B. Chi, J. Pu, J. Li, J. Power Sources 183 (2008) 586–589.
[17] Y.Y. Huang, J.M. Vohs, R.J. Gorte, J. Electrochem. Soc. 151 (2004) A646–A651.
[18] X. Liu, D. Han, H. Wu, X. Meng, F. Zeng, Z. Zhan, Int. J. Hydrogen Energy 38 (2013) 16563–16568.
[19] P. Blennow, J. Hjelm, T. Klemenso, A.H. Persson, S. Ramousse, M. Mogensen, Fuel Cells 11 (2011) 661–668.